Natural fractures at depth in the Lower Cretaceous Kuqa Depression tight sandstones: identification and characteristics

Tao Nian[1,2] , Yanze Li[3], Tao Hou[4], Chengqian Tan[1,2] and Chao Liu[1,2]

[1]School of Earth Sciences and Engineering, Xi'an Shiyou University, Xi'an, Shaanxi, 710065, China; [2]Shaanxi Key Laboratory of Petroleum Accumulation Geology, Xi'an, Shaanxi, 710065, China; [3]Jidong Oilfield Company, PetroChina, Tangshan, Hebei, 063000, China and [4]Huabei Oilfield Company, PetroChina, Renqiu, Hebei, 062552, China

Abstract

The Kuqa Depression in the northern Tarim Basin, NW China, is characterized by fault-controlled anticlines where natural fractures may influence production. Natural fractures in the Lower Cretaceous tight sandstones in the depression have been studied using seismic profiles, borehole images, cores and thin-sections. Results show that thrust faults, two types of opening-mode macrofractures and two types of microfractures are present. Thrust faults were generated during Cenozoic N–S-directed tectonic shortening and have hydraulically linked Jurassic source rocks and Cretaceous sandstones. Opening-mode fractures can be subdivided on the basis of sizes, filling characteristics and distribution patterns. Type 1 macrofractures are barren or mainly calcite-lined. They have straight traces with widths (opening displacements) that are of the order of magnitude of 10 μm, suggesting that their primary role is that of migration channels. Type 2 macrofractures are calcite-filled opening-mode fractures. They have an elliptical or tabular shape with sharply tapering tips. Transgranular microfractures are lens-shaped and open or filled mostly by calcite; maximum widths range between 0.01 mm and 0.1 mm. Intragranular microfractures are the most common microfracture type. They are filled by calcite, feldspar or quartz. The macrofractures and transgranular microfractures have regular distributions, while most intragranular microfractures are irregularly distributed owing to their inherited origin. The results imply that natural fractures in the tight sandstones were formed as tectonic, diagenetic and natural hydraulic origins. *In situ* stress and cementation analyses suggest that Type 1 macrofractures and their genesis-related microfractures have controlled the present flow system of the tight sandstones.

1. Introduction

Faults and opening-mode fractures can influence oil/gas migration (Bredehoeft & Norton, 1990, pp. 27–41; Cumella & Scheevel, 2008, pp. 137–55), groundwater transport (Gudmundsson, 2000), magma migration (Gudmundsson, 2011, pp. 525–52) and heat transfer (Pruess, 1983; Ghassemi & Kumar, 2007; Shaik *et al.* 2011), and engineering operations such as outcomes of hydraulic fracture treatments (Gale *et al.* 2018) and effective waste disposal (SD Ware *et al.* unpub. data, 1996; Figueiredo *et al.* 2016).

For tight sandstone reservoirs (matrix permeability less than 0.1×10^{-3} μm²; e.g. Dutton *et al.* 1993, p. 221), accurate characterization and prediction of fractures could be used to optimize well drilling and completion (Almansour *et al.* 2019) and potentially minimize the environmental footprint of oil/gas production. However, a key question is, what geological factors govern producibility from these rocks? Natural fractures have long been recognized as widespread features in tight sandstones (e.g. Laubach, 2003; Solano *et al.* 2011, and references therein). Studies show that fractures are present in tight sandstones in China (Zeng & Li, 2009; Lyu *et al.* 2017; Gong *et al.* 2019). Among the circumstances favouring fracture in these rocks are brittleness (Zeng & Li, 2009) and processes promoting fracture, such as tectonism and hydrocarbon generation and migration (e.g. Fall *et al.* 2015). It has also long been recognized that fractures, including those in tight sandstones, can form as a result of many different processes (loading paths) (e.g. Engelder, 1985; Pollard & Aydin, 1988; Laubach *et al.* 2019). Some of these processes produce fracture arrays having a wide range of sizes (e.g. Hooker *et al.* 2014) although some result in arrays with narrow size ranges (Laubach *et al.* 2016). Large-sized macrofractures can be observed by unaided eyes and small-sized microfractures are characterized fully using optical and electron microscopy techniques.

In this study, we aim to take the Lower Cretaceous Kuqa Depression tight sandstones as an example to depict natural fractures in macro- and microscopic views and further understand their distribution patterns in tight sandstones at depths more than 6500 m. The studied
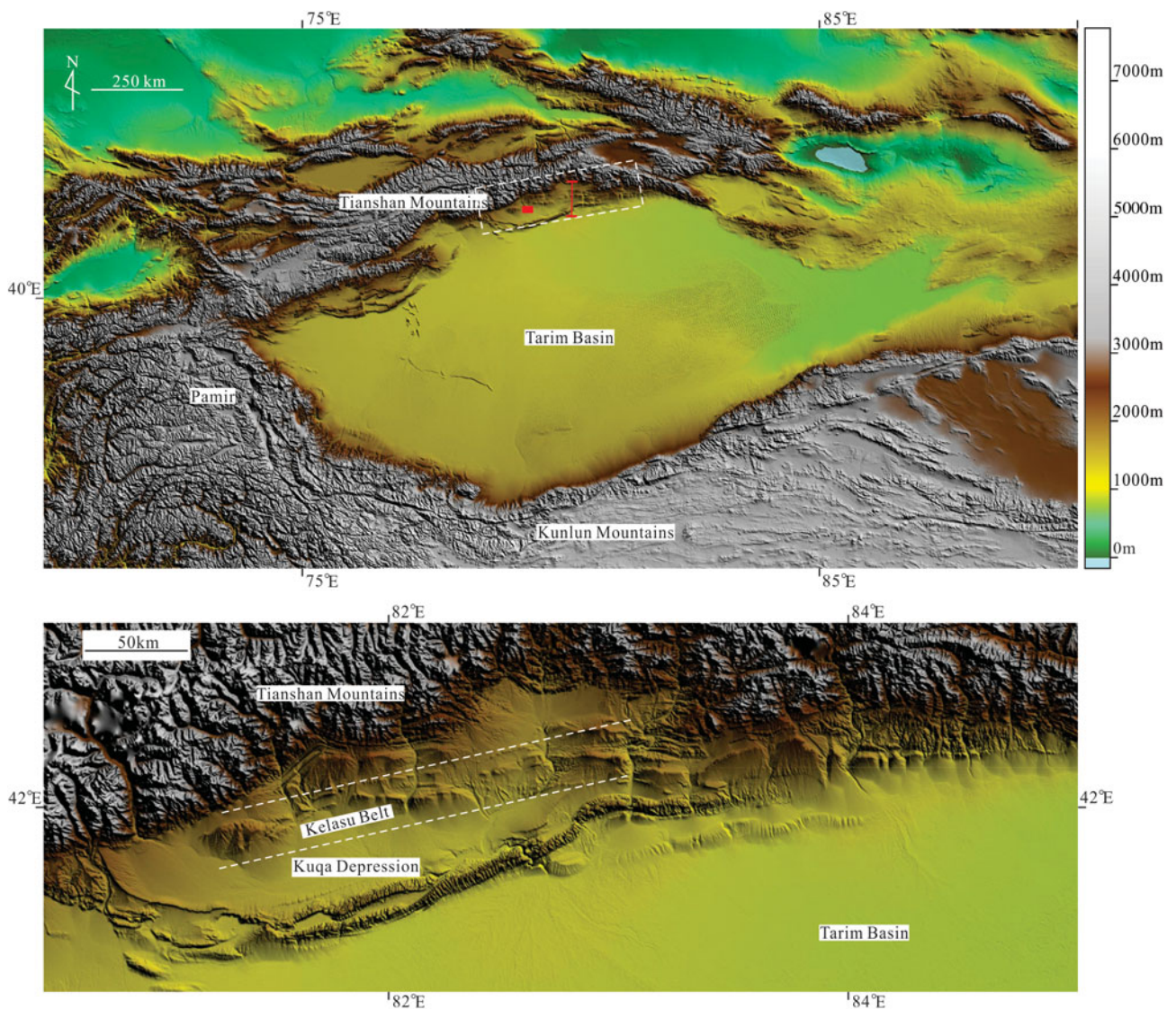
Fig. 1. (colour online) Location of the Kuqa Depression in the Tarim Basin, NW China (the dotted box). The red box and line represent location of the studied outcrop and the seismic line, respectively.

formation was classified as typical tight sandstones with matrix permeability varying between 0.01 mD and 0.1 mD (Zhang *et al.* 2014), and natural fractures have dominated flow of natural gas within the formation (Zhang *et al.* 2011; Yang *et al.* 2013; Qu *et al.* 2016; Liu *et al.* 2017). Previously, considerable studies have concentrated on macrofracture observation in outcrops and cores and suggested that these fractures were formed during the strata bending, and outcrop surveys reveal that at least one pair of conjugate shear fractures with high dip-angles could be the main fracture pattern in the tight sandstones (Zhang *et al.* 2012; JP Wang *et al.* 2014; Sun *et al.* 2015; Liu *et al.* 2016; ZY Wang *et al.* 2016); microfractures were barely mentioned except they have been noticed recently with the help of microscopic techniques (Liu *et al.* 2017).

Here, using cores, borehole images, thin-sections and an analogous outcrop selected in the Suohan area of the Kuqa Depression, we show that thrust faults, two types of macrofractures and two types of microfractures have been identified in the deep-seated tight sandstones. They are interpreted as tectonic, diagenetic or natural hydraulic fractures on the basis of spatial distribution

patterns, fracture morphology, orientations and mechanical properties. Their contributions to fluid flow are obviously different imprinted by *in situ* stresses or diagenetic processes which have modified flow capability of the fracture network. In combination with gas charge history in the tight sandstones, the main contributory fractures for the formation of the giant gas fields in the depression are also determined.

2. Geological setting

The Kuqa Depression in the Tarim Basin is adjacent to the Tianshan Mountains (Fig. 1) and is characterized by numerous thrust faults and fault-related anticlines with approximately west–east trends (Fig. 2). The thrust activity is related to the India–Asia plate collision during the Cenozoic (Guo *et al.* 1992, pp. 1–8; Lu *et al.* 1999; Liu *et al.* 2000). Crustal shortening derived from the plate collision propagated northwards in the Miocene, reactivating the older continental suture of the Tarim–Yili plate (Liu *et al.* 2000). This thrust movement in the Kuqa Depression is ongoing from the onset of the intracontinental collision to the
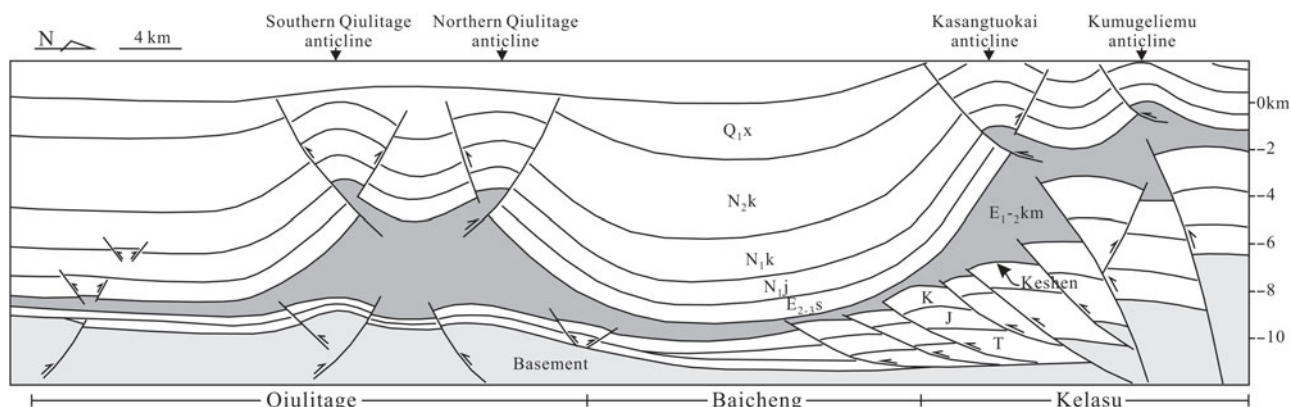
Fig. 2. The structural style across the central Kuqa Depression based on seismic interpretation (Neng *et al.* 2013). The seismic line is indicated in Figure 1. The letter "K" means the target Cretaceous sandstones; the characters "E$_{1-2}$km" represent the overlying Palaeogene halite and gypsum associations.

present (Liu *et al.* 2000; Wang *et al.* 2002). Two deformation modes during the movement have been proposed: one in which deformation is intermittent with a long-term dormancy between episodes of shortening (Wang *et al.* 2002); another involving one continuous contractional movement marked by a successive southward propagation (Liu *et al.* 2000; Zhang *et al.* 2003). Current tectonic activity in the area is great, marked for example by earthquakes Ms ≥ 5 that have occurred 62 times during the last ten years.

Mesozoic and Cenozoic stratigraphy in the Kuqa Depression is listed in Figure 3. The target Lower Cretaceous sandstones are surrounded by the overlying Palaeogene halite and underlying Cretaceous and Jurassic coal beds. During deposition of the sandstones, an arid climate prevailed (Jiang *et al.* 2008). Controlled by three depositional provenances including Northern Tianshan, Southeast Kuluketage and Southwest Wensu uplift (Chen *et al.* 2012), the target area successively developed fan deltas and braided-river deltas (Jia, 2000; Zhu *et al.* 2000). Drilling indicates that most of the petroleum wells encounter the braided-river deltas, in which siltstone and fine sandstone interbedded with thin mudrock are dominant rock types (Jia, 2000; Zhu *et al.* 2000; Gu *et al.* 2001). The high-frequency lateral migration of the braided-river deltas resulted in extensive sandstone deposits with sand/total ratios generally more than 95 % (Zhu *et al.* 2000).

Additionally, the sandstones have undergone complex diagenetic processes (Zhang *et al.* 2008, 2014). Early compaction and cementation mainly occurred at shallow depths (syngenetic to eogenetic stage) (Zhang *et al.* 2014). Porosity loss and formation tightness is a consequence of subsequent compaction derived from the burial of the formation to 6500 m depth and cementation mainly with calcite (Zhang *et al.* 2008, 2014). Moreover, compressive stresses generated from the Tarim–Yili plate collision may have increased the formation tightness to some extent (Shou *et al.* 2003; Li *et al.* 2009; Han *et al.* 2015). Petrophysical experiments at overburden conditions based on full-diameter cores and core plugs show that there is a good correlation between matrix porosity and permeability (Fig. 4). The target formation shows a low matrix porosity and permeability. The matrix porosity present varies between 0.76 % and 10.43 %, averaging 3.86 %, and the permeability ranges between 0.00007 mD and 0.49 mD, with 0.013 mD on average. Mercury injection tests indicate that the pore throats vary between 0.006 μm and 6.5 μm and the average value is 0.044 μm (Fig. 5).

3. Observation methods

3.a. Data collection

The seismic interpretation was conducted by researchers from the Tarim Oilfield Company, PetroChina. An outcrop was selected for survey in the west part of the Kuqa Depression (Fig. 1). The outcrop has a well exposed area of more than 5 km^2. The outcrop meets criteria set by Ukar *et al.* (2019) as a suitable analogue for the subsurface fractures. The total lengths of the cores are 150.2 m (492.8 ft) obtained at depths between 6500.0 m and 8035.0 m from seven vertical wells. Altogether, 336 stained thin-sections, 117 cathodoluminescence (CL) samples, 46 scanning electron microscope (FESEM/ SEM) samples and laser scanning confocal microscope (LSCM) samples were collected from these cores and analysed. In addition, 47 wells have measured borehole image log data with a total length of 13452.3 m, and the data were processed by standard procedure (Schlumberger, 2015).

3.b. Cores and image logs

The cores and the processed borehole images were used to depict macrofracture attributes including fracture morphology, orientations and distribution patterns. Fracture morphology further includes fracture surface textures, filling characteristics, terminations and cross-cutting relationships. Orientations refer to fracture dip angle and dip direction to horizontal planes or to the stratigraphy. Distribution pattern means fracture grouping and the spatial distribution of different fracture sets. The surface textures and filling characteristics were described using the cores. Other properties except fracture azimuth were obtained by the combination of cores and borehole images. The cores were calibrated to the borehole images (core shift) to determine the azimuths of the opening-mode unfilled or partially filled fractures in cores; and our observations indicate that fully calcite-filled fractures were rarely identified by image logs, hence the azimuths of the fully filled fractures can be deduced according to the spatial arrangement between the fractures and their adjacent unfilled or partially filled fractures or the corresponding bedding. The spatial distribution pattern in the subsurface is determined on the basis of outcrop analogues (Zhang *et al.* 2012; JP Wang *et al.* 2014; Sun *et al.* 2015; Liu *et al.* 2016; ZY Wang *et al.* 2016; this article), and core-image integration. Fracture morphology also provides key mechanical information to analyse their mechanical causes.
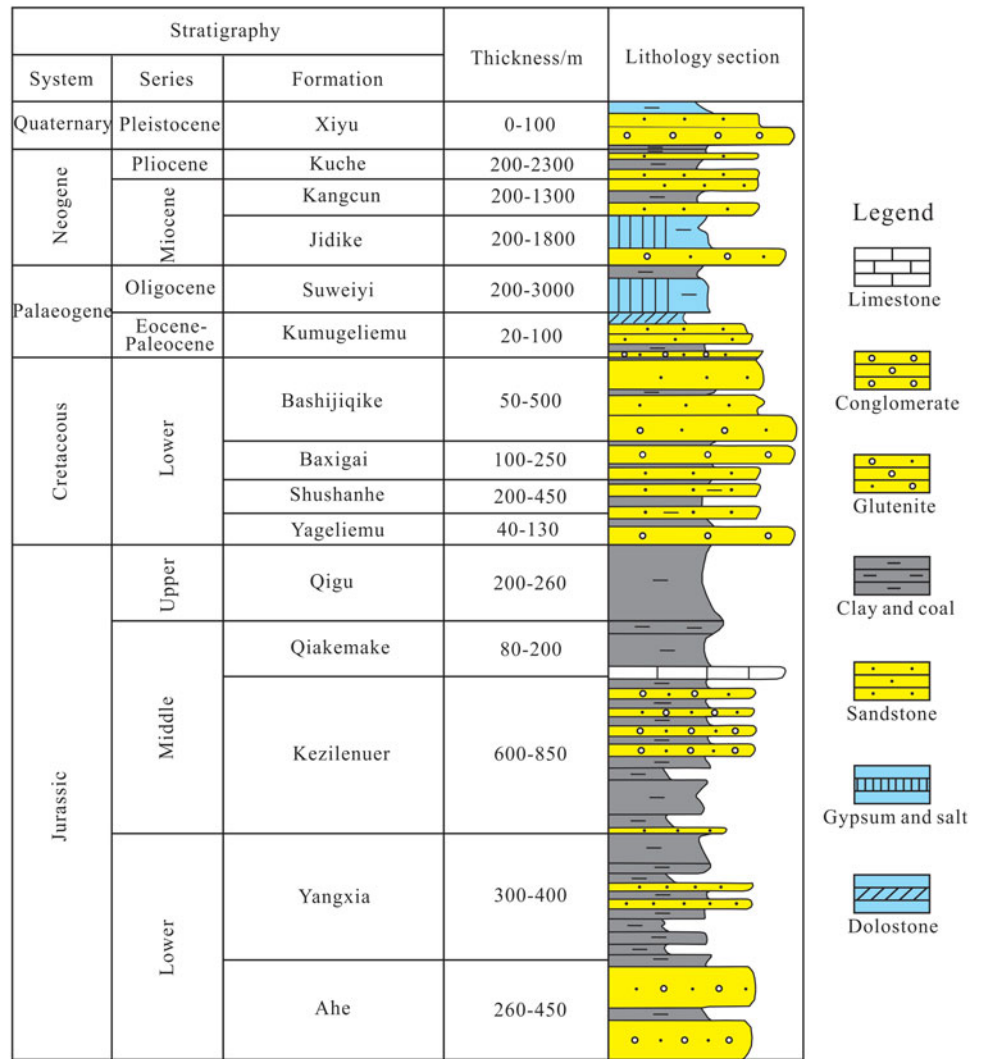
Stratigraphy			Thickness/m	Lithology section
System	Series	Formation		
Quaternary	Pleistocene	Xiyu	0–100	
Neogene	Pliocene	Kuche	200–2300	
	Miocene	Kangcun	200–1300	
		Jidike	200–1800	
Palaeogene	Oligocene	Suweiyi	200–3000	
	Eocene-Paleocene	Kumugeliemu	20–100	
Cretaceous	Lower	Bashijiqike	50–500	
		Baxigai	100–250	
		Shushanhe	200–450	
		Yageliemu	40–130	
Jurassic	Upper	Qigu	200–260	
	Middle	Qiakemake	80–200	
		Kezilenuer	600–850	
	Lower	Yangxia	300–400	
		Ahe	260–450	

Legend:
Limestone, Conglomerate, Glutenite, Clay and coal, Sandstone, Gypsum and salt, Dolostone

Fig. 3. (colour online) Stratigraphic column of the Mesozoic and Cenozoic in the Kuqa area (modified from Zhao *et al.* 2005).
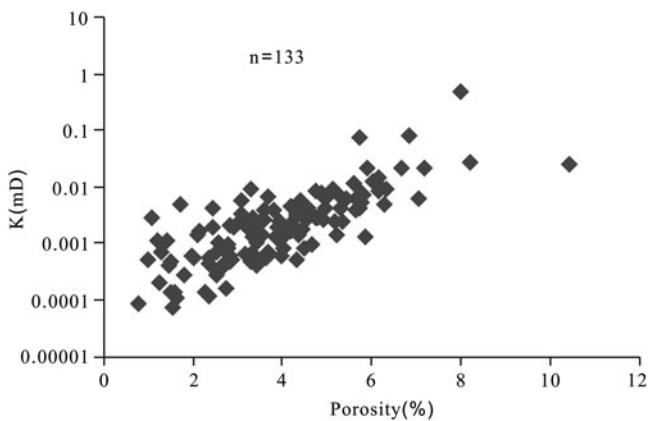

Fig. 4. Relationship between the matrix permeability and porosity in the tight sandstones.
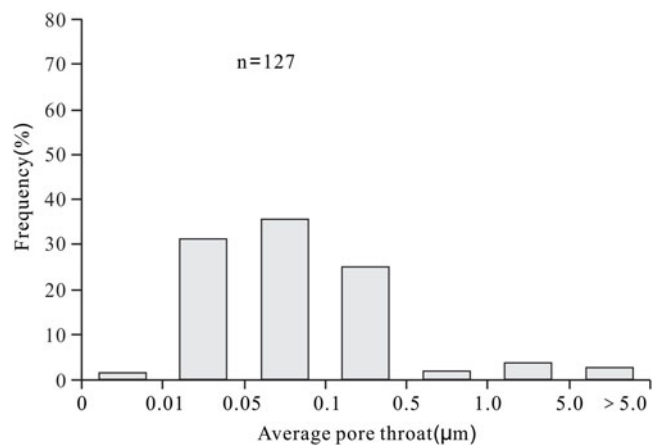

Fig. 5. Histogram showing the pore throat characteristics in the target formation.

3.c. Thin-sections

Thin-sections were used to describe microfracture morphology, orientations and distribution patterns. The attributes described match those recorded for the macrofractures. Most of the thin-sections were sampled in a specific direction parallel, perpendicular or oblique to depositional lamina. The sampling intervals gradually decreased close to one macrofracture. Stained thin-sections were impregnated with red epoxy resin. Additionally, seven thin-sections sampled from Type 2 macrofractures were also prepared and used for fluid inclusion observation,
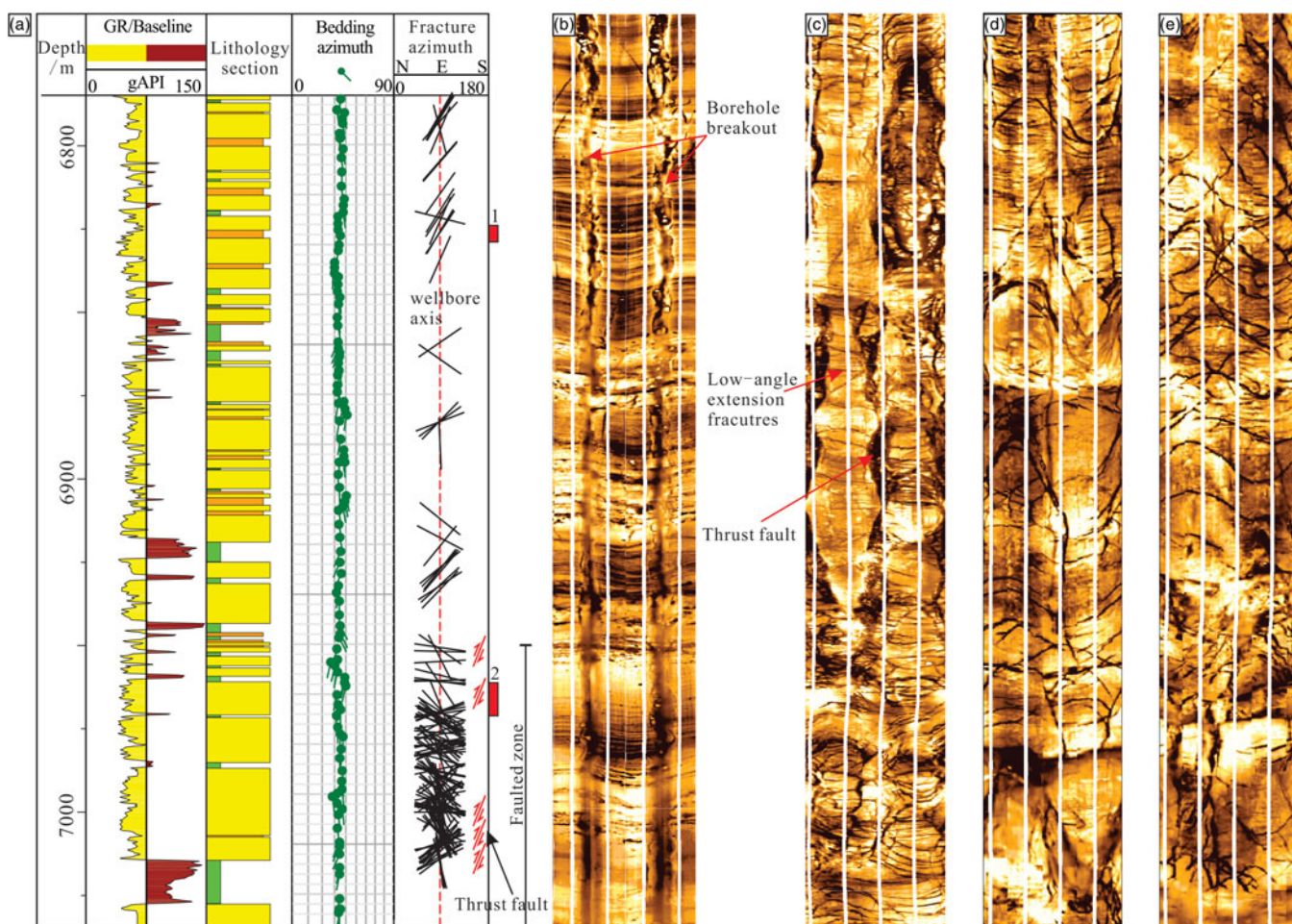
Fig. 6. (colour online) (a) Comprehensive stratigraphic column in one of the studied wells; the stratigraphic and fracture attitude are shown, respectively. (b) Typical borehole electrical images with normal fracture density; the image depth is marked with number 1 (the red box). (c, d, e) Successive images in the faulted zone. The depth of the images is marked with number 2 (the red box). Note that the bedding attitudes and lithology associations show minor variations from the top to the bottom imaged interval, while a distinctive boundary appears at 6950 m depth, below which fracture density increases abruptly along with thrust faults obliquely cutting through the wellbore. We speculate that two sets of the fractures with either west- or east-dip direction are related to local faulting activities. Another set of fractures with dip angles less than 10° has been documented from the vicinity of the potential fault zone, which corresponds to extension fractures.

and the homogenization temperatures were further measured on the basis of a standard workflow (Fall & Bodnar, 2018, and references therein).

4. Results

4.a. Thrust faults

A population of reverse faults in the subsurface, having middle to high dip angles, is identified in the seismic profile and shows imbricate characteristics (Fig. 2). Their vertical offsets range from 100 m to 500 m, with almost N–S-directed shortening. The thrust faults terminate downward within the underlying Jurassic coal or Triassic lacustrine mudrocks or intersect the basement downwards or thick salt deposits upwards (Fig. 2). Based on fault sizes, these thrust faults can be divided into two groups that develop at the tectonic unit boundaries, or within the sandstones (Fig. 6). The large-scale faults have restrained the dimensions of the gas pools and simultaneously act as gas pathways for migration from the source rock to the sandstones.

4.b. Macrofractures

The target sandstones contain two types of opening-mode macrofractures. The first type of fracture is open and superficially appears barren (no mineral fillings). For some of these, close inspection shows that some of the fractures are lined by small, faceted mineral crystals (e.g. calcite). Most of the second type of fracture are fully filled typically by calcite, but sometimes in wide fractures they can also show trace porosity if the larger fracture space is not completely filled.

4.b.1. Type 1: barren or mineral-lined opening-mode fractures
Barren or slightly mineral-lined fractures are developed within the sandstones, with high dip angles that vary between 52° and 86°. A total of 36 fractures were observed in the cores, and most have straight, sharp traces and relatively smooth surfaces (Fig. 7a). Microscopic observations show that the frequent offset grains on the opposite fracture walls impart a micrometre rugosity, suggesting they are opening-mode fractures. Core observation shows that the fractures are unbounded as in outcrops (Hooker *et al.* 2013) and

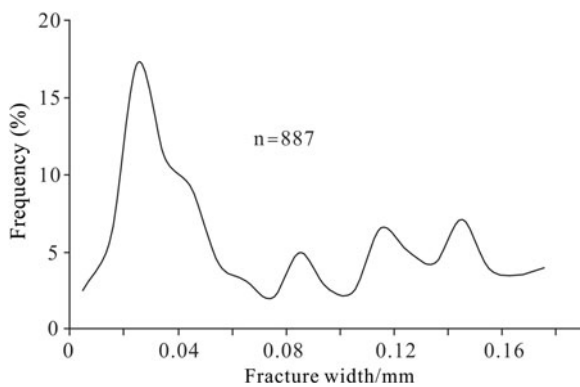**Fig. 7.** (colour online) Core photographs in the tight sandstones.

Fig. 8. The width distribution of Type 1 macrofractures in the sandstones; data are obtained from image logs and are highly skewed to the small end.

can propagate across thin mudrock layers with a thickness generally within 30 cm. The outcrop surveys show that their lengths are normally more than 5 m (Wang *et al.* 2014; this study), so the fractures always cut through core pieces and extend into the surrounding rocks.

The fracture widths are extremely small and are difficult to measure precisely. Image logs of the 887 fractures indicate that the average fracture widths range from 0.01 mm to 0.18 mm, and show a skewed distribution (Fig. 8). The fractures are porous, with the fracture porosity ranging between 0.01 % and 0.05 %, but locally lined with scattered mineral particles such as calcite (Fig. 7b), quartz or gypsum. Where the fracture space occurred with this mineral cement, mineral particles generally tend to form isolated deposits that bridge fracture walls. The fracture porosity

was calculated using the Monte Carlo method, which is associated with fracture widths and lengths and numbers of fractures present in samples (Howard & Nolen-Hoeksema, 1990).

In terms of the fracture distribution patterns, four sets of fractures are generally observed in the cores and borehole images (Fig. 9), whereas one set of fractures is poorly developed in the outcrops (Fig. 10). Two sets of the fractures commonly show conjugate features (Figs. 10, 11). Although no diagenetic evidence was found in the fractured cores, the cross-cutting relationships indicate the two sets of fractures should have formed at the same time. Combined with the fracture morphology, this poorly cemented opening-mode fracture could be formed as shear origins. The other two sets of fractures may be formed due to the minor variation of remote stress orientations. The orientations of the subsurface fracture sets are varied along with the structural positions, and show a potential distribution pattern (Fig. 9). Each set of fractures has a relatively consistent strike and a narrow strike range (Figs. 9, 10).

4.b.2. Type 2: fully filled opening-mode fractures

Another population of opening-mode fractures are entirely filled, mostly with calcite (Fig. 7c), e.g. they are veins. Minor wider, larger-sized fractures can contain trace to moderate residual pore space marked by euhedral calcite crystals, and the amount of pore space decreases towards fracture tips. A total of 96 fractures were observed in the cores, with dip angles mainly varying between 50° and 89° to horizontal planes, and most tabular-shaped fractures are perpendicular to bedding. In core cross-section, Type 2 fracture profiles are either tabular or elliptical with sharply tapering tips. Most fractures in the cores terminate at some bedding-parallel surfaces, such as lithology boundaries between mudrock and sandstone, or fabric boundaries between different sedimentary
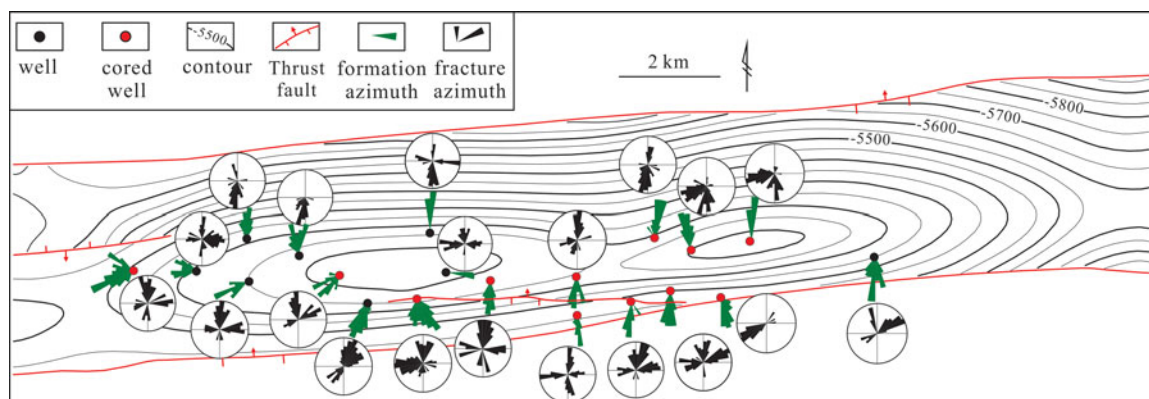
Fig. 9. (colour online) Type 1 fracture distribution patterns identified in the Keshen faulted anticline; the fracture and fault data are derived from borehole imaging and seismic interpretation, respectively. Along with variation of the stratum attitude, the fracture dip-directions show a slight rotation.
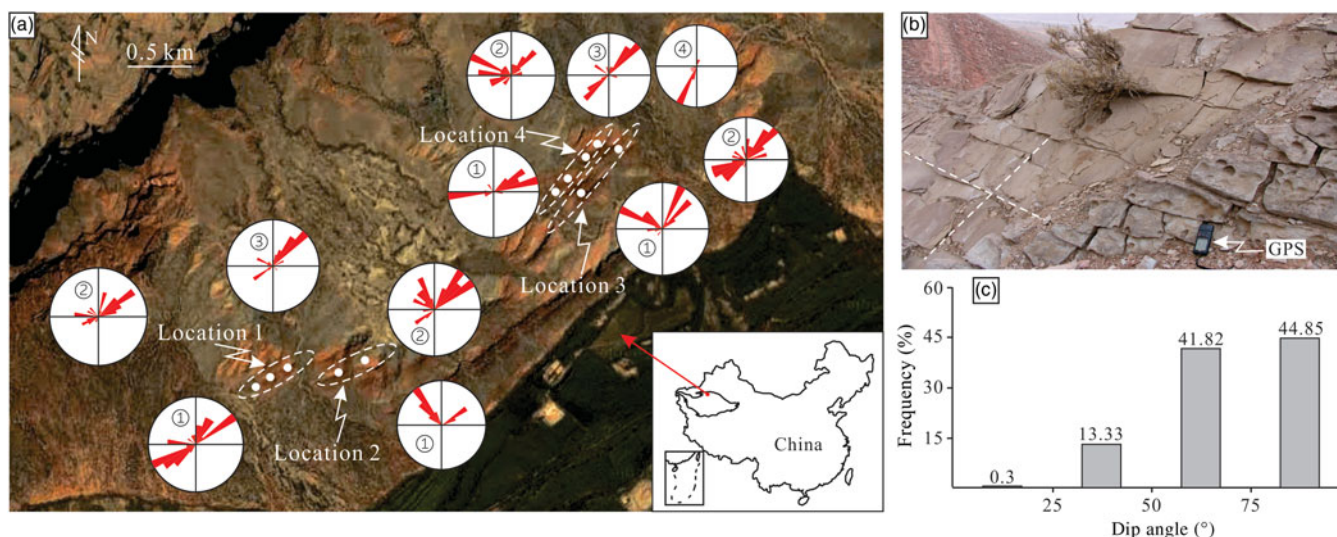
Fig. 10. (colour online) (a) The field survey locations and the corresponding fracture set dip-directions. The field survey was conducted by the Tarim Oilfield Company, PetroChina. The outcrop sandstones are comparable to the subsurface because they have similar fold shapes and tectonic evolution history. (b) One pair of typical conjugate fractures in the tight sandstones; the fractures have a maximum length up to 5 m. The GPS is 172 mm length. (c) Histogram showing distribution of the fracture dip angles, mostly ranging between 45° and 90° in the outcrops.

structures, or scoured surfaces, which means they are bed-bounded as in outcrops (Hooker *et al.* 2013).

The widths (opening displacements) of Type 2 filled fractures can be accurately measured, and these fractures have maximum widths varying between 0.2 mm and 5 mm, typically less than 2.5 mm. Maximum width means the maximum distance between two fracture walls along fracture trace. This value could show a good linear relation with the fracture height in the majority of Type 2 fractures; however, some of the fractures also exhibit non-linear features in which a smaller width can correspond to a larger fracture height. In combination with fracture shapes, the former is formed as tension or extension fractures corresponding to elliptical shape (Vermilye & Scholz, 1995), and the latter may be originally formed under shear stress and lately filled or they may be hybrid fractures corresponding to tabular appearance. The height-to-maximum-width ratios of the elliptical fractures are 40–270, whereas they are 400–1100 in tabular fractures.

The sediments were in an alkaline diagenetic setting, and calcite is the main diagenetic cement (Zhang *et al.* 2014). The fractures having enough space are filled mostly with calcite (Fig. 12), which shows obvious chemical reaction with hydrochloric acid. Some tabular-shaped fractures can also be filled with calcite and/or carbon showing multilayer fabrics where calcite is closely adjacent to fracture walls and carbon is filled adjacent to the early calcite; the late calcite precipitate is filled at the fracture centre (Fig. 13a).

The elliptical-shaped fractures have a relatively consistent N–S strike, with dispersion within 20°. They are basically perpendicular to horizontal planes (relative to wellbore axis direction), and lack any obvious geometrical relationships with the hosting beds. Lack of the cross-cutting and abutting relations suggests that their sets generally could not be determined by tectonic analysis. Core observation also shows that these fractures are principally concentrated at the top of the anticlines. Additionally, a population of mineral-filled microfractures develops parallel to the fractures, which resemble the macrofractures in shape and distribution patterns. The tabular fractures are approximately perpendicular to hosting bedding and dip steeply. Their orientations are commonly consistent with one set of fractures in Type 1.

Fig. 11. (colour online) Conjugate fracture pairs in the borehole image and cores. (a) The processed electrical image having two sets of fractures with the opposite dip-directions. (b) Core pieces with conjugate fracture pairs, calibrated to the corresponding borehole image; the core shift process can be seen in Nian *et al.* (2016). (c) Two sets of conjugate fractures in the core; the white staining along the fracture traces suggests that fractures are serving as conduits to fluid flow.
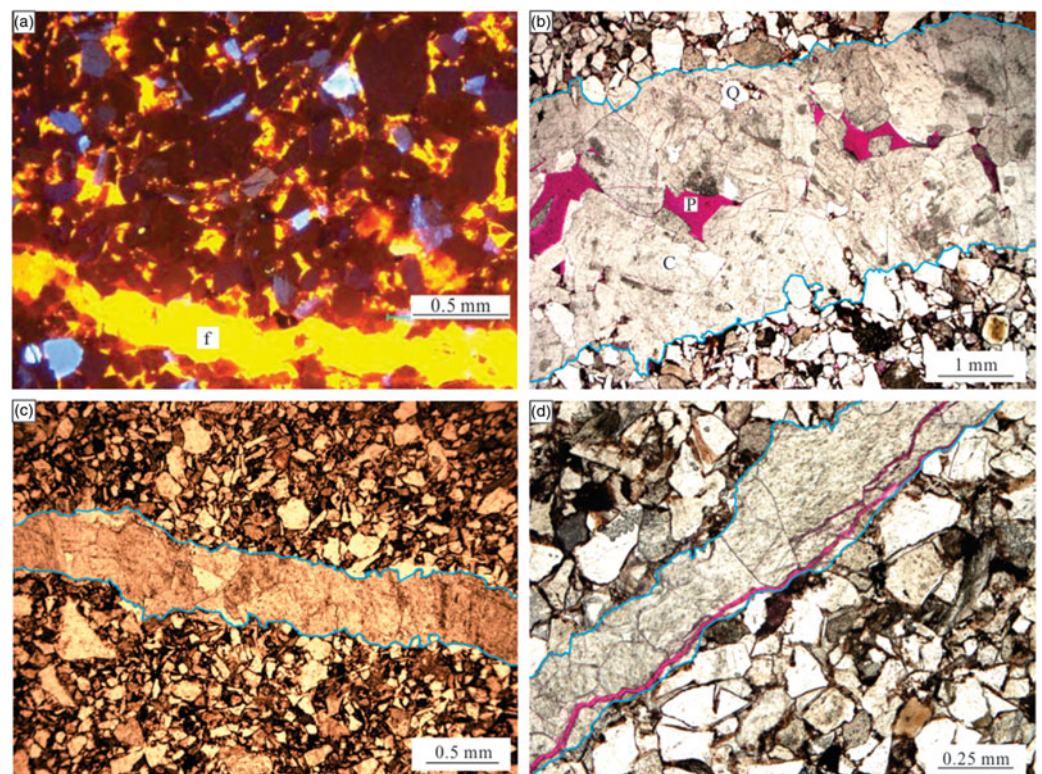

Fig. 12. (colour online) (a) CL image sampled from 6766 m core, showing a section of a macrofracture filled by calcite. Brown, blue, orange and yellow colour represent quartz, feldspar, dolomite and calcite, respectively. (b) A 3 mm wide macrofracture filled by calcite (C); multiple xenomorphic calcite grains can be identified through their cleavages with different strikes. Quartz grains (Q) from hosting rocks are captured and distributed in the vicinity of fracture walls (between the two blue lines). Fracture pore space (P) is filled by stains, stained thin-section, 6618.1 m. (c) A 0.5 mm wide macrofracture, 6987.0 m. (d) A 0.25 mm wide macrofracture filled by calcite; two open microfractures are later developed along and adjacent to the macrofracture wall, respectively, 6567.7 m.
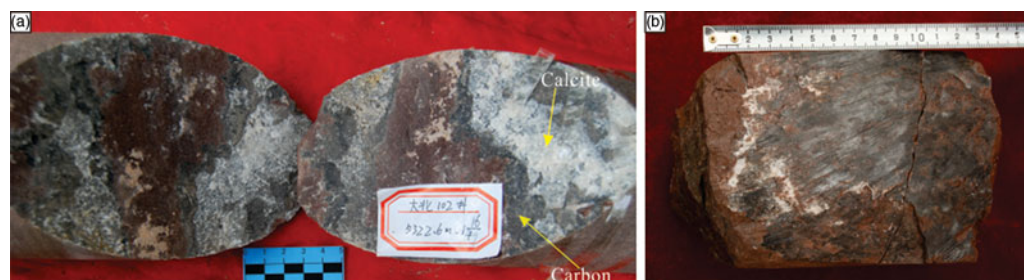
Fig. 13. (colour online) Macrofracture fabrics filled by calcite and carbon. (a) Calcite precipitated after carbonization. (b) Calcite precipitated before carbonization.
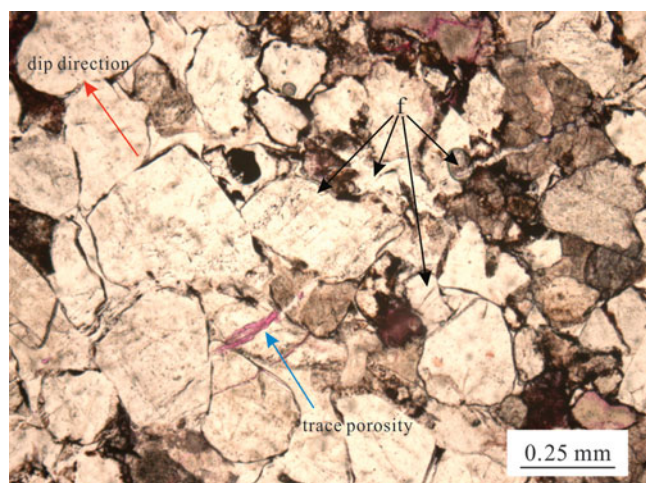
Fig. 14. (colour online) Transgranular microfractures in the tight sandstones, revealed by stained thin-sections sampled in the vicinity of the macrofractures in Figure 7c. The formation dips nearly (342°) to the north, and the microfractures are almost perpendicular to the bedding. A relatively wider transgranular microfracture cuts across grains, and is primarily calcite-filled but locally contains trace porosity (the red stain). Several smaller transgranular fractures with similar orientations are also developed.

4.c. Microfractures

4.c.1. Transgranular fractures

Transgranular fractures are microfractures with fracture widths less than 0.1 mm and having lengths of millimetres or less (Anders *et al.* 2014); or they have aspect-ratios commonly varying between 10^2 and 10^5 (Simmon & Richter, 1976, pp. 105–37; Kranz, 1983). Transgranular microfractures in the sandstones are displayed via different type of thin-sections, and refer to fractures cutting across multiple grains and intergranular cement (Fig. 14), indicating that the rock has been cemented and indurated when the fractures grew. A total of 462 transgranular microfractures were observed with lens-shaped appearance. The microfracture trace is generally straight with no severe deviation along fracture trajectory, although locally deflecting at boundaries of grains such as feldspar, quartz and debris. The fractures generally have dip angles varying between 50° and 90°.

Owing to their elliptical appearance, the width of a single transgranular fracture is a variable and continually varied along its fracture trace, thus decreaseing to zero at fracture tips. The apparent maximum fracture width was measured via thin-sections. Although the true fracture width should be measured in thin-sections perpendicular to fracture profile, most thin-sections are commonly oblique to fracture profile to some extent. Thus, the measured apparent microfracture widths tend to be larger and

need to be corrected by the angle between hosting thin-section and the fracture profile. The calculation shows that the maximum widths of the transgranular microfracture are varied between 0.01 mm and 0.1 mm, and exhibit a good linear relation with the corresponding fracture heights, indicating that the transgranular fractures could be Mode I fractures. The fractures have height-width ratio of 65–300.
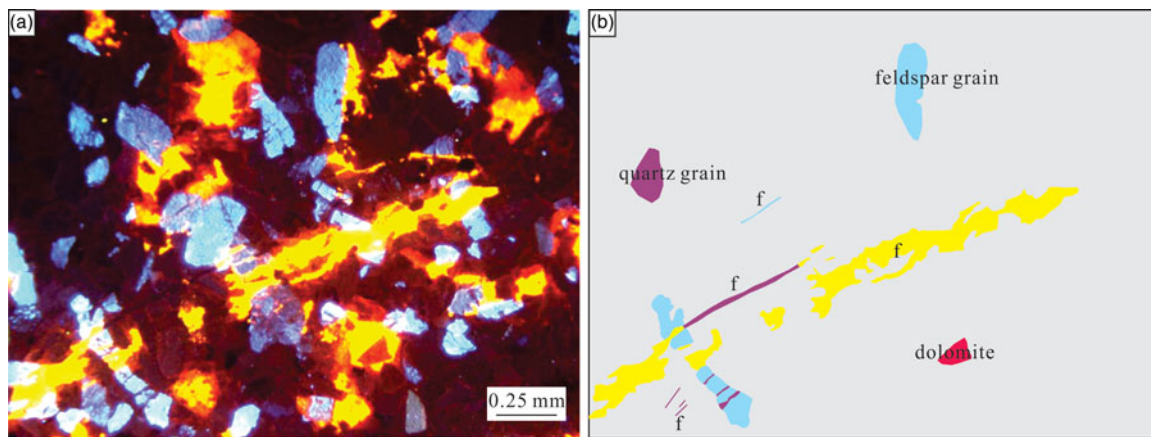
Not all the transgranular fractures are fully or partly filled by diagenetic minerals, and if the precipitation occurred, most of the filling minerals are calcite (Fig. 15); the fractures can also be filled with quartz and feldspar. Crack-texture is not common within the fracture space. The early-filled fractures can be partly dissolved with residual pore space, indicating that they have a certain connectivity degree. The total fracture porosity changes between 0.1 % and 0.6 %, and could be increased by more than 0.3 % when abundant transgranular fractures are aggregated.

Most unfilled transgranular microfractures are preferentially aligned and show approximately the same fracture sets as Type 1 macrofractures in the same bed, although with a relatively wide direction range (Fig. 16a, b). These microfractures show strikes that match one of their nearby macrofractures. The microfractures could have a distance to their nearest-neighbour macrofractures, which suggests that they are not all in close proximity to the neighbour macrofractures. Microscopic observation further indicates that late-formed microfractures are more easily induced within macrofractures and their fracture walls (Fig. 12d).

Some transgranular fractures are frequently observed at the lithologic boundaries between mudrock and sandstone, or within mudrock layers (Fig. 17). As long as mudrock deposits are present, one can see this type of microfracture always occurred. These fractures are barely filled with minerals and generally show a relatively fresh fracture morphology, which suggests they were newly formed. The fracture width varies between 0.01 mm and 0.04 mm. The porosity varies between 0.05% and 0.2%. These microfractures develop closely along beddings (thus parallel to the beddings), where layers bend, end, pinch or branch (Zeng, 2010; this study).

4.c.2. Intragranular fractures

The vast majority of microfractures sampled within the tight sandstones are **i**ntragranular, signifying that their fracture tips lie within or coincident with detrital grains. In reality, they are small in contrast to the transgranular fractures and widely distributed in the sandstones, and can be observed in almost every thin-section with sufficient resolution. The LSCM observation shows that the fracture profiles are elliptical with sharply tapering tips when two fracture tips terminate within mineral grains; otherwise they are straight and have distinct or indistinct boundaries probably in case of the fluid inclusions. The fractures also occasionally appear as triangular-shaped if one fracture tip taper closes at grain

Fig. 15. (colour online) CL image of the transgranular fractures and the corresponding image interpretation. (a) CL image showing development of quartz, feldspar, dolomite and calcite. The fracture space has a crack-seal texture and is mostly filled with calcite, though with quartz and feldspar precipitates. (b) Interpretation of (a).

contacts and the other terminates at the opposite grain edge, and tend to exhibit maximum width.

The widths of intragranular fractures are obtained on the basis of the CL, LSCM and FESEM/SEM section. Each fracture's width is extremely small and we estimate the maximum width of the intra-granular fractures should be at a 10 μm order of magnitude. The minimum width range is likely near several nm. The height-width aspect ratios are various. The elliptical-shaped are between 50 and 350, consistent with Type 2 macrofractures and transgranular fractures, whereas the straight-shaped are 300–800. The fracture porosity ranges between 0.01 % and 0.4 %.

Intragranular fractures may seal rapidly. Most intragranular microfractures are filled with calcite, feldspar or quartz (Fig. 18a), suggesting that they poorly conduct natural fluids. The microfracturing and cementation may be concurrent events, though insufficient evidence is provided here. Overall, the fractures display a wide range in direction (Fig. 16c) probably owing to the multiple fracturing origins occurring before, during and after dep-osition. Thus, the distribution patterns of intragranular fractures are also various and related to the fracture origins (discussed below). However, they generally initiate at point and line contacts between portions of grain boundaries. According to their spatial arrangement with mineral grains, these fractures are identified within quartz, feldspar and other grains in the sandstones, and they commonly appear as fracture swarms.

# 5. Discussion

5.a. Fracture genesis

Natural fractures are formed with tectonic loading (e.g. Stearns, 1968, pp. 97–118; Stearns & Friedman, 1972, pp. 82–106; Engelder 1985; Cooper *et al.* 2006; Lacombe *et al.* 2011), overpres-sure (Handin *et al.* 1963; Secor, 1965, 1969, pp. 3–47; Fall *et al.* 2015) or diagenetic compaction (Zeng & Li, 2009; Zeng, 2010). Fracture genesis is notoriously difficult to pin down. This is because sedimentary basins generally have experienced complex tectonic evolution, and diverse subsidence, thermal and fluid-flow histories, spanning tens to hundreds of millions of years, and every process could be responsible for fracturing (Laubach and Ward, 2006). Moreover, paths of fracturing derived from these various origins may coincide over geological time.

In combination with tectonic loading, formation pressure evolution, and burial history in the studied sandstones, these macro- and microfracture origins are interpreted based on their morphology, orientations, mechanical properties and spatial distribution patterns.

5.a.1. Tectonic fractures

Tectonic fractures are those whose origin can be attributed to regional or local tectonic events. The thrust faults are formed dur-ing the regional N–S-directed shortening (Neng *et al.* 2013). Several clues are integrated to verify that Type 1 macrofractures together with tabular-shaped Type 2 fractures are the most certain to have formed owing to bed folding or faulting. In terms of spatial arrangements, fractures formed during fold growth have a specific geometric relationship with the folds (Stearns, 1968, pp. 97–118). Type 1 macrofractures are barren and not influenced by cementa-tion, which implies they are formed during late syn-folding. According to the adjacent outcrop surveys in the same sandstone formations, a similar fracture distribution pattern compared to the subsurface was observed. The cross-cutting and abutting relations indicate that these fractures are two conjugate fracture pairs and their formation could be controlled by two stages of regional com-pression with horizontal maximum stress orientation changed from early NNW–SSE to late N–S (Zeng *et al.* 2004; Wang *et al.* 2014), with a deflection angle *c*. 25°. Accordingly, the stresses were characterized with a vertical intermediate stress and a greatest compressive stress parallel to the dip direction of bedding. Moreover, syn-folding fracture sets can be specifically related to bedding, and their attitudes could change spatially, for instance, at the nose of an anticline, where the direction of greatest curvature changes (Bergbauer & Pollard, 2004); thus it interprets why the fracture attitudes seem to vary along with the structural position and bedding. Some recent significant studies further argued that occurrence of pre-folding fractures or pre-folding deformation structures can change the common view of fold-fracture rela-tions (Bergbauer & Pollard, 2004; Ahmadhadi *et al.* 2007, 2008; Amrouch *et al.* 2010; Lacombe *et al.* 2011; Beaudoin *et al.* 2012; Tavani *et al.* 2015). Considering the orientations of the thrust movement were not obviously varied during the Cenozoic and the orientations of tabular-shaped Type 2 fractures are basically consistent with one set of fractures in Type 1, we speculate that
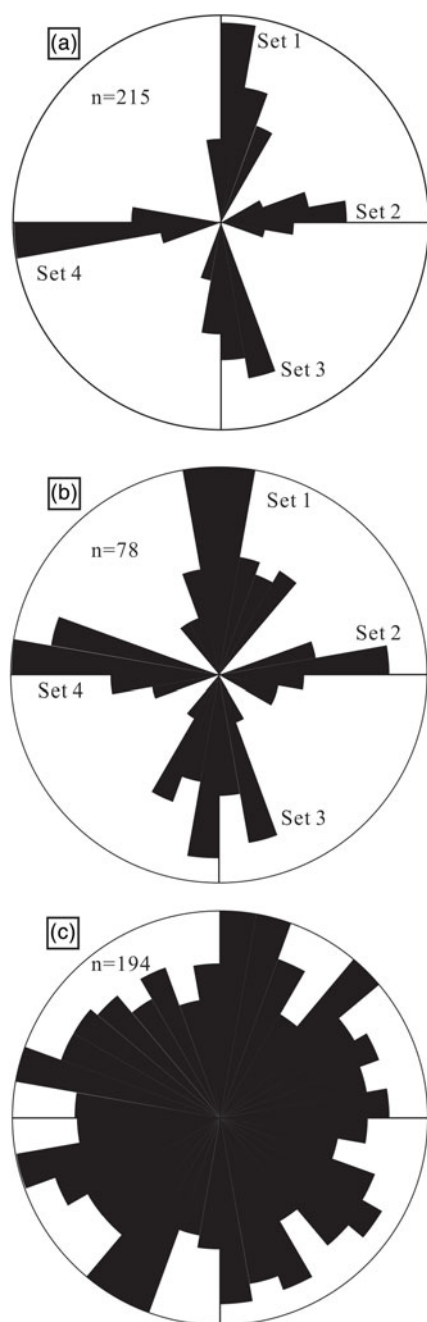
Fig. 16. Rose diagrams of fracture dip-directions in one of the cored wells (core length 17.9 m). (a) Type 1 macrofractures; the data were calculated from 220 m imaging log; (b) their adjacent transgranular microfractures; the data were obtained from stain thin-section and the CL technique; and (c) their adjacent intragranular microfractures; the data were measured using the FESEM/SEM and the LSCM technique.

these fractures could be formed during early syn-folding and subjected to cementation later.

For tabular-shaped Type 2 fractures filled by calcite and/or carbon, one interpretation is that open fractures first filled with calcite in the early stage. However, before the fractures were fully filled by calcite, oil migrated into the sandstone formation (23–12 Ma; Liang *et al.* 2002; Zhao *et al.* 2002; Lu *et al.* 2012). During the subsequent subsidence accompanied by the lateral compressive stress related to the Southern Tianshan Orogen (12–5.5 Ma; Zhang *et al.* 2008, 2014), oil in the fractures began to carbonize, thus occurring

with sliding friction. This event is manifested by the striations along the carbon-layer surfaces (Fig. 13b). Eventually, the fractures reopened under the local stress field and were filled by late calcite cement (*c.* 5.5 Ma; Zhang *et al.* 2008, 2014).

Fault planes accommodate shear displacement and there are three sets of potential fracture swarms, with one set of shear fractures parallel to the fault plane, one set of shear fractures conjugate to the fault plane and one set of extension fractures bisecting the acute angle of these two sets of shear fractures (Nelson, 2001, p. 13). The majority of tectonic fractures in the studied formation were produced in association with the folding process, and their fracture density, the number of fractures per metre of vertical core or wellbore, is generally less than 0.8 fractures per metre. However, fractures are extremely dense in local concentrations and variably oriented. Three other sets of fractures are generally developed and interpreted as tectonic fault-related fractures on the basis of their distribution patterns (Fig. 6). These fault-related fractures are important for the *in situ* stress analysis, fault prediction and fluid flow. Additionally, the majority of transgranular fractures have a similar orientation and dip angle distribution to Type 1 macrofractures or tabular-shaped Type 2 fractures, and are interpreted as smaller members of the same fracture set (Laubach & Ward, 2006; Hooker *et al.* 2009). As in the discussion above, Type 1 and tabular-shaped Type 2 macrofractures are identified as tectonic fractures, therefore most transgranular fractures are of tectonic origin.

Although the origin of most intragranular fractures is difficult to determine in deformed tight sandstones, some must have formed during tectonic movement based on their fracture spatial patterns which are related to a certain regional or local tectonic stress (Fig. 19). Other properties, such as fracture morphology and filling characteristics, are generally difficult to use to determine the fracture origin. In reality, the origins of intragranular fractures could be more easily determined in undeformed strata; if a stratum has ever been subjected to tectonic deformations and original orientations of intragranular fractures have been rotated, their genesis is generally difficult to deduce. For instance, formation of the intragranular fractures with a radial pattern in the sandstones is related to intense crushing and grain-scale stress concentrations at grain-contact points (Laubach & Ward, 2006). The compressive stress can be gravity or tectonic stresses. Generally, it is difficult to judge the fracture origin unless the stratum can be recovered to its undeformed state. In an idealized case, if the fracturing propagation path is nearly vertical, intragranular fractures could be deduced formed by diagenetic compaction to some extent; otherwise they may be tectonic microfractures.

5.a.2. Diagenetic fractures

Diagenetic fractures in tight sandstones mainly result from physical diagenesis (Zeng, 2010), such as compaction, and most are intragranular fractures specifically attributable to grain crushing (Laubach, 1997; Milliken and Laubach, 2000, pp. 225–43). These microfractures are identified as being of diagenetic and not tectonic origin, integrating their distribution patterns, shapes and fracture timings. The most intense fracturing induced by diagenetic compaction in the sandstones should have occurred during the Neogene (Zhang *et al.* 2008, 2014), when the formation was buried from 2400 m to 6500 m during *c.* 20 Ma (Fig. 20). The vertical stress derived from the overburden weight already changes between 150 MPa and 160 MPa at present. The CL observation shows that almost all the intragranular fractures were sealed with authigenic minerals. Lander & Laubach (2015) propose that this

Fig. 17. (colour online) Diagenetic fractures along the mudrock layers in stained thin-sections. (a) Calcite partially precipitated in the fracture space (dotted circles), indicating the fractures are naturally formed. (b) The fractures are bending and directionally extending coincident with the adjacent bedding plane (the lower bedding).
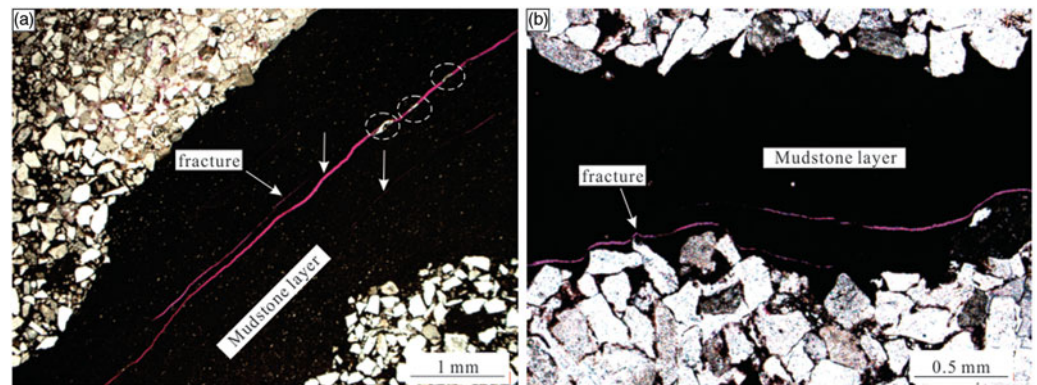
Fig. 18. (colour online) (a) Filled intragranular fractures in the CL image (line or latticed feature), 7011.4 m. (b) A rich array of inherited intragranular fractures are developed in the quartz (Q) and feldspar (F) grains, and filled by minerals, stained thin-section, 6357.4 m. The intragranular fractures show radial patterns indicating that they initiated at grain contacts, but the contacts feature and corresponding initiation point (IP) no longer exist.
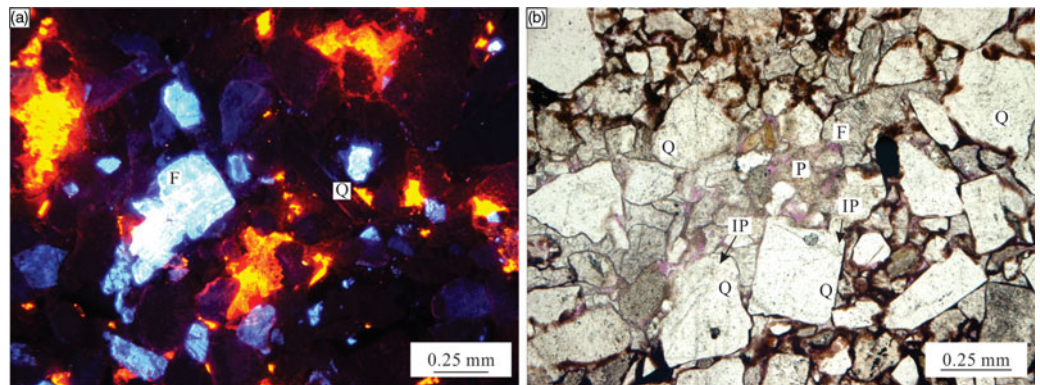
Fig. 19. (colour online) Stained thin-section containing the tectonic microfractures (a) and the corresponding image interpretation (b). The section is cut along horizontal bedding. The intragranular fractures formed first, or at least simultaneously with the two transgranular fractures (partially filled), and most show a sub-parallel feature with the transgranular fractures.
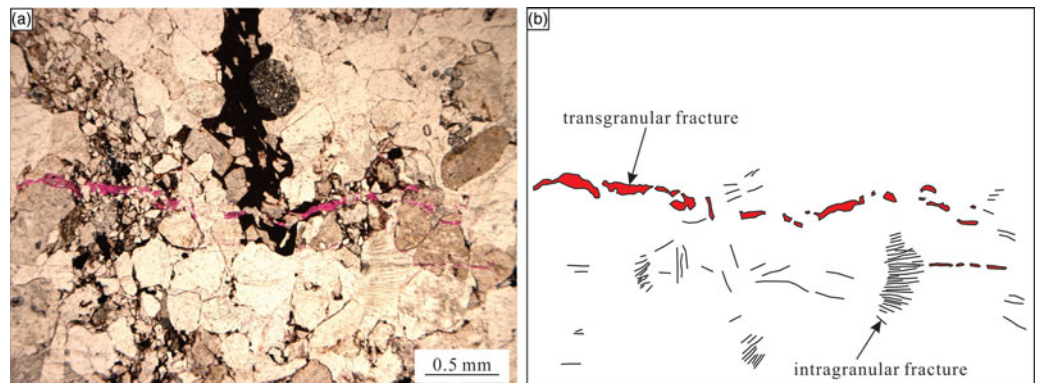
occurs because minerals like quartz may preferentially precipitate on low-energy surfaces of microfractures due to their smooth and planar features. Here, homogenization temperatures could provide a good estimate for true trapping temperatures; we have analysed the homogenization temperature of fluid inclusions in some selected intragranular fracture fillings and they formed coincident with the period of rapid subsidence (Fig. 20).

A large portion of intragranular microfractures should be inherited and transported from a sediment source area on the basis of shapes and patterns. The microfractures do not show an intact elliptical, tabular or wedge shape, but show a sharp line feature within grains, and the fractures are truncated at grain boundaries. These inherited fractures end at grain edges and do not cross into intergranular cement (Fig. 18b). The fractures can have orientations and patterns, but these could not be used to identify their origins.

5.a.3. Natural hydraulic fractures

Natural hydraulic fractures (NHFs) are induced by elevated pore pressure, which reduces effective normal stress (Handin *et al.* 1963; Secor, 1965; 1969, pp. 3–47). The occurrence of an overpressured environment and natural hydraulic fractures in the tight sandstones studied here is based on several preconditions, although researchers still held different ideas on the main controlling factors of abnormally high pressure (Zeng & Liu, 2006). First, multiple salt layers, with a total thickness generally more than 400'm, were deposited above the tight sandstones during the Palaeogene (Fig. 2; Pi *et al.* 2002; Zeng & Liu, 2006; Wang, 2014; Wang *et al.* 2015). These impermeable layers can provide a good capping condition for the subsequent fluid accumulation. Second, the studied sandstone formation has been subjected to long-term tectonic compression during the Neogene and Quaternary period (Pi *et al.* 2002; Zeng & Liu, 2006). The
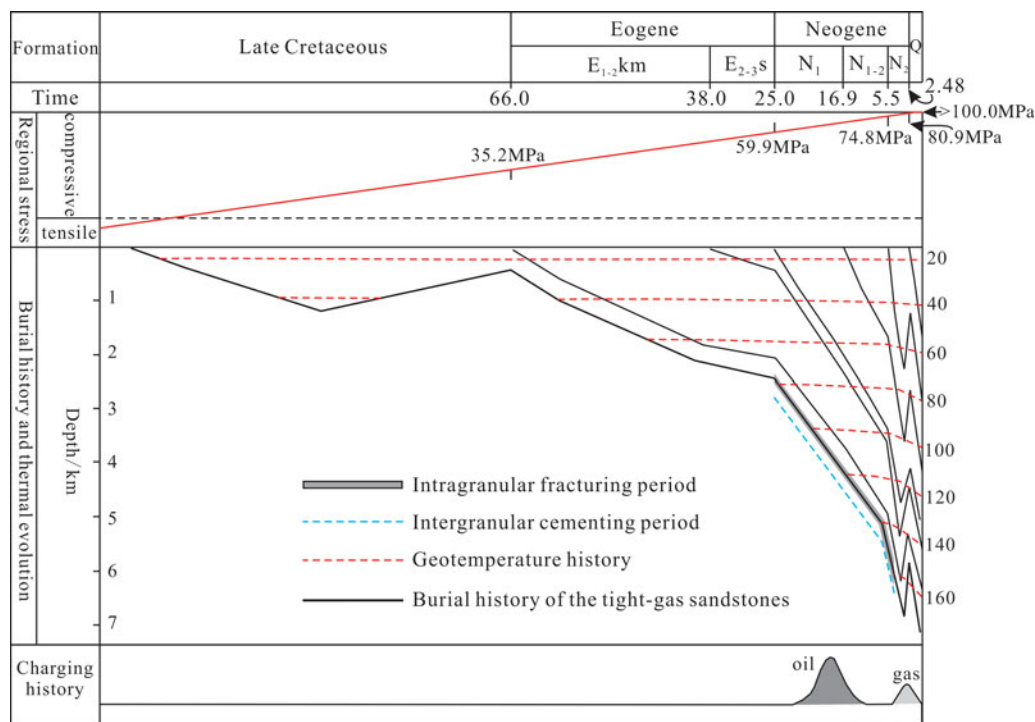
Fig. 20. (colour online) Burial history, geotemperature history, palaeo-tectonic stress and oil/gas charging history, and fluid-inclusion homogenization temperature of quartz deposit in the intragranular (within quartz grains) fractures. The burial history was recovered using compaction correction and back-stripping technique (Zhang *et al.* 2014). Geotemperature history was obtained by simulation using vitrinite reflectance data. Palaeo-tectonic stress is obtained using rock acoustic emission from Zeng *et al.* (2004). The charging history is referred from Liang *et al.* (2002). The absolute stratigraphic age is determined by Jia (2004). A total number of 117 homogenization temperature data is collected from Yuan *et al.* (2015) and Mao *et al.* (2015).

overburden pressure experiment, simulating the tight sandstone core samples subjected to tectonic stresses similar to the subsurface environment, indicates that *c.* 76 % of the crustal stress would be reduced by pore fluid pressure when the maximum horizontal principal stress (SHmax) exceeds 34 MPa (Zeng & Liu, 2006), which also suggests that strong tectonic compression could contribute to the formation of overpressure. Third, the formation pressure difference between the Jurassic source rock and the tight sandstones was commonly more than 70 MPa (Wang *et al.* 2015), and forced the fluid continuously charging from the source rock to the sandstone reservoirs. Overall, the thrust movement, combined with overlying salt layers and high-pressure fluids injected from the underlying source rocks, has resulted in an overpressured environment in the sandstones.

In the mentioned fracture types, elliptical-shaped Type 2 fractures and their genetic-related transgranular fractures are interpreted as natural hydraulic fractures. They are developed at the top of the anticlines, and the tensile shape indicates they are veins of the products of tension stress. In the cores, they extend parallel to the borehole axis, and well correlation suggests these fractures lack a geometrical relationship with depositional beds. The macrofractures are perpendicular or sub-perpendicular to the minimum principal stress; thus they are NHFs probably formed as oil migrated into the sandstone formation, and a positive opening corresponds to a negative effective stress (Zeng, 2010; Anders *et al.* 2014).

5.b. Fracture timing

Determination of fracture timing in naturally fractured formations is difficult due to complex fracture swarm containing multiple origins of fractures which formed during a long geological history. At the early stage, relative fracturing timing is determined mainly on the basis of cross-cutting and abutting relationships. Use of cement deposits in fracture space and their fluid inclusions further

allows a relatively accurate determination of fracture timing (Fall *et al.* 2012, 2015). Moreover, utility of U–Pb dating on calcite cements of natural fractures can more accurately constrain the formation time of these fractures and reveal complex stress evolution and deformation sequences (Beaudoin *et al.* 2018).

The thrust faults have orientations and displacement patterns that are kinematically consistent with compressional deformation of Southern Tianshan orogen. Tectonic analysis based on outcrop survey and seismic interpretation indicates that they have formed since the Miocene (Liu *et al.* 2000). Type 1 macrofractures are newly formed because the fracture surface is barren and moderately or weakly influenced by diagenesis, which suggests they are younger than Type 2 fractures within the same bedding. Our estimated homogenization temperatures of fluid inclusions contained within infills of Type 2 elliptical macrofractures indicate that this type of fracture began to form in the Early Neogene, with fluid-inclusion homogenization temperatures *c.* 80°C to 90°C, while the palaeogeotherm derived from oxygen isotopes of the tabular macrofractures changes between 85°C and 130°C (JP Wang *et al.* 2014; Wang, unpub. data, 2015). Therefore, according to the burial and geotemperature curves (Fig. 20), Type 2 fractures were mainly formed during the Early to Middle Neogene (from 25.0 Ma to 11.0 Ma).

Although lacking fluid inclusion data, a few relations can be investigated to determine relative fracture timing in the microfractures. Most of the transgranular fractures, as we discussed, are tectonic fractures formed related to Type 1 macrofractures or tabular-shaped Type 2 macrofractures. Macrofractures are generally the result of the coalescence of microfractures (Mogi, 1962; Tham *et al.* 2005). Therefore, the transgranular fractures with barren surfaces could be formed prior to Type 1 macrofractures and the filled transgranular microfractures were probably formed prior to tabular-shaped Type 2 macrofractures. The cross-cutting and abutting relationships between the transgranular microfractures and other types of fracture are absent. Homogenization

temperatures of the fluid inclusions or oxygen isotopes in the inherited fractures have not been specially measured, but they formed before occurrence of the deposition. Some early diagenetic fractures were formed along with the early subsidence corresponding to the palaeogeotemperature less than 80°C (Yuan *et al.* 2015), and other intragranular fractures were mainly formed from 25.0 Ma to 5.5'Ma (Fig. 20).

5.c. Implications for gas migration

The multiple-origin natural fractures developed within the tight sandstones have played specific roles during oil/gas flow from the source layers to the sandstone reservoirs, or between the adjacent sandstone layers. However, they can not only increase formation permeability, but also decrease formation permeability when natural fractures are diagenetically filled.

As discussed above, the imbricate faulted fractures have linked the Jurassic coal-bearing source rocks and the target sandstone reservoirs. In combination with the petroleum charging characteristics (He *et al.* 2009; Wang, 2014; Fig. 20), they are significant channels during the primary gas migration since *c.* 2.48 Ma (Fig. 20; Wang, 2014). Driven by the abnormally high pressure generated within the source rock, natural gas can migrate in the vertical and lateral directions along these faults (He *et al.* 2004; Li & Liu, 2009; Wang, 2014), and finally formed the well-known gas pools in China, such as the Kela2 and Keshen. The vertical migration distance commonly varies between 2 km and 5 km.

When the oil and gas fluid migrated out of the source rock and into the tight sandstones, the secondary migration started. The described fracture properties would to some extent influence fluid flow during this period. Given that the pre-existing parallel-plate model calculating fracture permeability indicates that the value is significantly related to fracture width (Huitt, 1955), it can be assumed that a single unfilled Type 2 macrofracture should be more hydraulically conductive than a Type 1 macrofracture. In reality, the presence of oil inclusions within the fracture infillings indicates Type 2 macrofractures always act as good migration channels for oil. The calculation also indicates that the transgranular microfractures are generally wider than intragranular fractures, suggesting that fluid would preferentially migrate via the transgranular microfractures. The widths of Type 1 fractures are sensitive to overburden pressure due to the fresh fracture surface which is not sealed or bridged by mineral particles. The values obtained from the imaging log indicate that their geometrical fracture widths would be less and probably near the order of magnitude of 10 μm considering the principle of width calculation based on image logs (Luthi & Souhaite, 1990). Therefore, Type 1 macrofractures may have a similar width range to the maximum widths of transgranular microfractures. In the deep subsurface formation, these two types of fracture should have similar influence to fluid flow considering the parameter of fracture width.

Type 2 macrofractures in these faulted anticlines are independent of the present stress direction, while the current dominant sets of open fractures are Type 1 fold-related fractures. As described above, they have moderate to high dip angle, indicating that the vertical stress may show a relatively weak effect on the fracture width and permeability. *In situ* maximum horizontal stress can control fracture permeability via its relationship with fracture strikes (Barton *et al.* 1995; Zeng & Li, 2009). The four sets of Type 1 fractures have different angles of intersection to the current SHmax orientation. The fractures striking approximately E–W are basically perpendicular to the direction of the SHmax (Zeng *et al.*

2004), and have a poor hydraulic conductivity, with an average permeability less than 1.3 mD (T. Nian, unpub. Ph.D. thesis, China Univ. of Petroleum, 2017), while Type 1 fractures with strikes parallel to or within 35° of the horizontal maximum principal stress often exhibit the most efficient passage for the largest volumes of gas flow according to the production test, and their average permeability varies between 2.2 mD and 10.1 mD (T.'Nian, unpub. Ph.D. thesis, China Univ. of Petroleum, 2017). Thus, a permeability anisotropy is commonly expected with maximum permeability orientations intersecting with corresponding SHmax orientation less than 35°. Additionally, the maximum permeability orientations are rotated in the hinge zones owing to the local variation of Type 1 fracture attitude. Moreover, the fault-related fractures could obviously enhance local formation permeability.

Diagenetic evolution indicates that the sandstone formation was subjected to two main cementation events, respectively corresponding to the syngenetic (before 66 Ma) and mesogenetic (from 16.9 Ma to 5.5 Ma) periods (Zhang *et al.* 2014). Hence, the fractures formed prior to the cementation show poor hydraulic conductivity; some of the filled Type 2 macrofractures and microfractures were dissolved in the late diagenetic history, but overall they show a low dissolution degree. Although these fractures with tectonic, overpressure and diagenetic origins have established a complicated fracture system which links different types of pore space, fractures developed after 5.5 Ma could be more conductive and provide the main channels for fluid flow in the sandstone formations present. Natural gas in the sandstones began to accumulate after the Pliocene (Zhao *et al.* 2002; Wang & Long, 2010; Lu *et al.* 2012). Therefore, Type 1 macrofractures and their related microfractures, which appear as multi-scale fracture swarms contributing to the formation permeability, are main gas migration channels within the sandstones. The open microfractures connect the intergranular- and intragranular pores, and Type 1 macrofractures link the sandstone layers, thus resulting in the widely distributed gas pools in the Kuqa Depression.

6. Conclusions

In this study, thrust faults, two types of macrofractures and two types of microfractures have been identified in the Lower Cretaceous Kuqa Depression tight sandstones. The thrust faults formed during the Cenozoic shortening and act as the primary migration channels linking the underlying Jurassic coal-bearing source rocks and the sandstone reservoirs. Type 1 macrofractures appear as fresh or locally mineral-lined and have a kinematic width probably near the order of magnitude of 10 μm in the deep subsurface, and the fracture porosity varies between 0.01 % and 0.05 %, suggesting they merely play the role of migration channels and do not significantly increase the total porosity. Type 2 macrofractures are fully mineral-filled fractures showing elliptical or tabular shape with sharply tapering tips. Their maximum fracture widths show a good linear relation to the elliptical-shaped fractures, with corresponding fracture heights which suggest they are formed under tension stress. The transgranular microfractures, with maximum widths varying between 0.01 mm and 0.1 mm, are open or filled mostly by calcite. Although the intragranular microfractures are the most developed, they are filled by calcite, feldspar or quartz and make no contribution to reservoir producibility. The macrofractures and transgranular microfractures are regularly distributed considering they were formed corresponding to folding/faulting processes, diagenetic compaction and naturally

hydraulic fracturing, respectively. Most of the intragranular microfractures are inherited with an irregular distribution. In combination with spatial arrangements, orientations, morphology and mechanical properties, these fractures can be divided into tectonic fractures (Type 1 macrofractures, tabular-shaped Type 2 macrofractures and related transgranular and intragranular fractures), diagenetic intragranular fractures, and natural hydraulic fractures (elliptical-shaped Type 2 macrofractures and related transgranular fractures). Their relative formation times are further determined based on tectonic and diagenetic analysis and fluid inclusion data. Analysis of diagenetic cementation and orientation relations with *in situ* stress field indicates that Type 1 macrofractures and their related microfractures have controlled the present flow system of the tight sandstones.

References

Ahmadhadi F, Daniel J-M, Azzizadeh M and Lacombe O (2008) Evidence for pre-folding vein development in the Oligo-Miocene Asmari Formation in the Central Zagros Fold Belt, Iran. *Tectonics* **27**, TC1016. doi: 10.1029/2006TC001978.

Ahmadhadi F, Lacombe O and Daniel J-M (2007) Early reactivation of basement faults in Central Zagros (SW Iran): evidence from pre-folding fracture populations in the Asmari Formation and Lower Tertiary paleogeography. In *Thrust Belts and Foreland Basins; From Fold Kinematics to Hydrocarbon Systems* (eds O Lacombe, J Lavé, J Vergès and F Roure), pp. 205–28. Berlin: Springer-Verlag.

Almansour A, Laubach SE, Bickel JE and Schultz RA (2019) Value of information analysis of a fracture prediction method. *SPE Reservoir Evaluation & Engineering*. doi: 10.2118/198906-PA.

Amrouch K, Lacombe O, Bellahsen N, Daniel J-M and Callot J-P (2010) Stress and strain patterns, kinematics and deformation mechanisms in a basement-cored anticline: Sheep Mountain Anticline, Wyoming. *Tectonics* **29**, TC1005. doi: 10.1029/2009TC002525.

Anders MH, Laubach S and Scholz CH (2014) Microfractures: a review. *Journal of Structural Geology* **69**, 377–94.

Barton CA, Zoback MD and Moos D (1995) Fluid flow along potentially active faults in crystalline rock. *Geology* **23**, 683–6.

Beaudoin N, Lacombe O, Roberts NMW and Koehn D (2018) U-Pb dating of calcite veins reveals complex stress evolution and thrust sequence in the Bighorn Basin, Wyoming, USA. *Geology* **46**, 1015–18. doi: 10.1130/G45379.1.

Beaudoin N, Leprêtre R, Bellahsen N, Lacombe O, Amrouch K, Callot J-P, Emmanuel L and Daniel J-M (2012) Structural and microstructural evolution of the Rattlesnake Mountain Anticline (Wyoming, USA): new insights into the Sevier and Laramide orogenic stress build-up in the Bighorn Basin. *Tectonophysics* **576–577**, 20–45.

Bergbauer S and Pollard DD (2004) A new conceptual fold-fracture model including prefolding joints, based on the Emigrant Gap anticline, Wyoming. *GSA Bulletin* **116**, 294–307.

Bredehoeft JD and Norton DL (1990) Mass and energy transport in a deforming Earth's crust. In *The Role of Fluids in Crustal Processes* (ed. National Research Council), pp. 27–41. Washington, DC: National Academy Press.

Chen G, Huang ZB, Zhang HL, Zhang RH and Yan XF (2012) Provenance analysis of clastic rocks in the Cretaceous Bashijiqike Formation in Kuqa Depression. *Natural Gas Geoscience* **23**, 1025–33.

Cooper SP, Goodwin LB and Lorenz JC (2006) Fracture and fault patterns associated with basement-cored anticlines: the example of Teapot Dome, Wyoming. *AAPG Bulletin* **90**, 1903–20.

Cumella SP and Scheevel J (2008) The influence of stratigraphy and rock mechanics on Mesaverde gas distribution, Piceance Basin, Colorado. In *Understanding, Exploring, and Developing Tight-Gas Sands* (eds SP Cumella, KW Shanley and WK Camp), pp. 137–55. AAPG Hedberg Series 3. Tulsa, OK: American Association of Petroleum Geologists.

Dutton SP, Clift SJ, Hamilton DS, Hamlin HS, Hentz TF, Howard WE, Akhter MS and Laubach SE (1993) Major low-permeability-sandstone gas reservoirs in the continental United States. The University of Texas at Austin, Bureau of Economic Geology Report of Investigations No. 211, 221 pp.

Engelder T (1985) Loading paths to joint propagation during a tectonic cycle: an example from the Appalachian Plateau USA. *Journal of Structural Geology* **7**, 459–76.

Fall A and Bodnar R (2018) How precisely can the temperature of a fluid event be constrained using fluid inclusions? *Economic Geology* **113**, 1817–43. doi: 10.5382/econgeo.2018.4614

Fall A, Eichhubl P, Bodnar RJ, Laubach SE and Davis JS (2015) Natural hydraulic fracturing of tight-gas sandstone reservoirs, Piceance Basin, Colorado. *GSA Bulletin* **127**, 61–75.

Fall A, Eichhubl P, Cumella SP, Bodnar RJ, Laubach SE and Becker SP (2012) Testing the basin-centered gas accumulation model using fluid inclusion observations: southern Piceance Basin, Colorado. *AAPG Bulletin* **96**, 2297–318.

Figueiredo B, Tsang CF, Niemi A and Lindgren G (2016) Review: the state-of-art of sparse channel models and their applicability to performance assessment of radioactive waste repositories in fractured crystalline formations. *Hydrogeology Journal* **24**, 1607–22.

Gale JFW, Elliott SJ and Laubach SE (2018) Hydraulic fractures in core from stimulated reservoirs: core fracture description of HFTS slant core, Midland Basin, West Texas. SPE/AAPG/SEG Unconventional Resources Technology Conference, URTEC-2902624-M. Houston, Texas, 23–25 July 2018. doi: 10.15530/urtec-2018-2902624.

Ghassemi A and Kumar GS (2007) Changes in fracture aperture and fluid pressure due to thermal stress and silica dissolution/precipitation induced by heat extraction from subsurface rocks. *Geothermics* **36**, 115–40.

Gong L, Su XC, Gao S, Fu XF, Jabbari H, Wang XX, Liu B, Yue WT, Wang ZS and Gao A (2019) Characteristics and formation mechanism of natural fractures in the tight gas sandstones of Jiulongshan gas field, China. *Journal of Petroleum Science and Engineering* **175**, 1112–21.

Gu JY, Fang H and Jia JH (2001) Diagenesis and reservoir characteristics of Cretaceous braided delta sandbody in Kuqa Depression, Tarim Basin. *Acta Sedimentologica Sinica* **19**, 517–23 (in Chinese with English abstract).

Gudmundsson A (2000) Active fault zones and ground water flow. *Geophysical Research Letters* **27**, 2993–6. doi: 10.1029/1999GL011266

Gudmundsson A (2011) *Rock Fractures in Geological Processes*. Cambridge: Cambridge University Press.

Guo LZ, Shi YS and Lu HF (1992) Two types of remote tectonic effect associated with India-Tibetan collision. In *Modern Geology Research* (eds QB Li, JX Dai, RQ Liu and JL Li), pp. 1–8. Nanjing: Nanjing University Press (in Chinese).

Han DL, Zhao RZ, Li Z and Li WF (2015) The characteristic of diagenetic compaction induced by multiform geodynamic mechanisms in reservoir: an example from Cretaceous sandstone reservoir in Kuqa Depression, Tarim Basin. *Chinese Journal of Geology* **50**, 241–8.

Handin J, Hager RV, Friedman JM and Feather J (1963) Experimental deformation of sedimentary rocks under confining pressure: pore pressure tests. *AAPG Bulletin* **47**, 717–55.

He DF, Zhou XY, Yang HJ, Lei GL and Ma YJ (2009) Geological structure and its controls on giant oil and gas fields in Kuqa Depression, Tarim Basin: a clue from new shot seismic data. *Geotectonica et Metallogenia* **33**, 19–32.

He GY, Lu HF and Li SX (2004) Petroleum migration features in the Kuqa rejuvenated foreland basin, northwestern China. *Acta Geologica Sinica* **78**, 848–53.

Hooker JN, Gale JFW, Gomez LA, Laubach SE, Marrett R and Reed RM (2009) Aperture-size scaling variations in a low-strain opening-mode fracture set, Cozzette Sandstone, Colorado. *Journal of Structural Geology* **31**, 707–18.

Hooker JN, Laubach SE and Marrett R (2013) Fracture-aperture size-frequency, spatial distribution, and growth processes in strata-bounded and non-strata-boundedfractures, Cambrian Mesón Group, NW Argentina. *Journal of Structural Geology* **54**, 54–71.

Hooker JN, Laubach SE and Marrett R (2014) A universal power-law scaling exponent for fracture apertures in sandstones. *GSA Bulletin* **126**, 1340–62.

Howard JH and Nolen-Hoeksema RC (1990) Description of natural fracture systems for quantitative use in petroleum geology. *AAPG Bulletin* **74**, 151–62.

Huitt JL (1955) Fluid flow in simulated fractures. *American Institute of Chemical Engineers Journal* **2**, 259–64.

Jia CZ (2004) *Plate tectonics and continental dynamics in the Tarim Basin.* Petroleum Industry Press, pp. 168–169.

Jia JH (2000) Depositional sequence and reservoir of Cretaceous Bashijiqike formation in Kuqa foreland basin. *Earth Science Frontier* **7**, 133–43 (in Chinese with English abstract).

Jiang DX, Wang YD and Wei J (2008) Palynoflora and its environmental significance of the Early Cretaceous in Baichen, Xinjiang Autonomous region. *Journal of Palaeogeography* **10**, 77–86 (in Chinese with English abstract).

Kranz RL (1983) Microcracks in rocks: a review. *Tectonophysics* **100**, 449–80.

Lacombe O, Bellahsen N and Mouthereau F (2011) Fracture patterns in the Zagros Simply Folded Belt (Fars, Iran): constraints on early collisional tectonic history and role of basement faults. *Geological Magazine* **148**, 940–63.

Lander RH and Laubach SE (2015) Insights into rates of fracture growth and sealing from a model for quartz cementation in fractured sandstones. *GSA Bulletin* **127**, 516–38. doi: 10.1130/B31092.1.

Laubach SE, Lander RH, Criscenti LJ, Anovitz LM, Urai JL, Pollyea RM, Hooker JN, Narr W, Evans MA, Kerisit SN, Olson JE, Dewers T, Fisher D, Bodnar R, Evans B, Dove P, Bonnell LM, Marder MP and Pyrak-Nolte L (2019) The role of chemistry in fracture pattern development and opportunities to advance interpretations of geological materials. *Reviews of Geophysics* **57**, 1065–1111. doi: 10.1029/2019RG000671.

Laubach SE, Fall A, Copley LK, Marrett R and Wilkins S (2016) Fracture porosity creation and persistence in a basement-involved Laramide fold, Upper CretaceousFrontier Formation, Green River Basin, USA. *Geological Magazine* **153**, 887–910.

Laubach SE and Ward ME (2006) Diagenesis in porosity evolution of opening-mode fractures, Middle Triassic to Lower Jurassic La Boca Formation, NE Mexico. *Tectonophysics* **419**, 75–97.

Laubach SE (1997) A method to detect natural fracture strike in sandstones. *AAPG Bulletin* **81**, 604–23.

Laubach SE (2003) Practical approaches to identifying sealed and open fractures. *AAPG Bulletin* **87**, 561–79.

Li Z, Zhang LJ, Shou JF, Han DL, Shen Y and Zhang HL (2009) Structural strain and structural heterogeneity of sandstone diagenesis: a case study of the Kuqa subbasin in the northern Tarim basin. *Acta Petrologica Sinica* **25**, 2320–30 (in Chinese with English abstract).

Li ZS and Liu DL (2009) Fault systems in Kuqa area, northern Tarim and its control to oil-gas accumulation. *Chinese Journal of Geology* **44**, 26–34.

Liang DG, Zhang SC, Zhao MJ and Wang FY (2002) Hydrocarbon sources and stages of reservoir formation in Kuqa Depression, Tarim Basin. *Chinese Science Bulletin* **47**, 62–70.

Liu C, Zhang RH, Zhang HL and Wang B (2016) Fracture development of different structural styles in Kuqa foreland thrust belt: from outcrop observation of structural fracture. *Natural Gas Geoscience* **28**, 1–10.

Liu C, Zhang RH, Zhang HL, Wang JP, Mo T, Wang K and Zhou L (2017) Genesis and reservoir significance of multi-scale natural fractures in Kuqa foreland thrust belt, Tarim Basin, NW China. *Petroleum Exploration and Development* **44**, 1–10.

Liu ZH, Lu HF, Li XJ, Jia CZ, Lei GL, Chen CM, Wang GQ and Fan XT (2000) Tectonic evolution of Kuqa rejuvenated foreland basin. *Scientia Geologica Sinica* **35**, 482–92 (in Chinese with English abstract).

Lu HF, Jia D, Chen CM, Liu ZH, Wang GQ and Jia CZ (1999) Nature and timing of the Kuqa Cenozoic structures. *Earth Science Frontiers (China University of Geosciences, Beijing)* **6**, 215–21 (in Chinese with English abstract).

Lu XS, Liu KY and Zhuo QG (2012) Palaeo-fluid evidence for the multi-stage hydrocarbon charges in Kela-2 Gas field, Kuqa foreland basin, Tarim Basin. *Petroleum Exploration and Development* **39**, 537–44 (in Chinese with English abstract).

Luthi S and Souhaite P (1990) Fracture aperture from electrical borehole scans. *Geophysics* **74**, 821–33.

Lyu WY, Zeng LB, Zhang BJ, Miao FB, Lyu P and Dong SQ (2017) Influence of natural fractures on gas accumulation in the Upper Triassic tight gas sandstones in the northwestern Sichuan Basin, China. *Marine and Petroleum Geology* **83**, 60–72.

Mao,YK, Zhong DK, Neng Y, Zhang CW, Liu YL, Wang A and Hu XL (2015) Fluid inclusion characteristics and hydrocarbons accumulation of the Cretaceous reservoirs in Kuqa foreland thrust belt, Tarim basin, Northwest China. *Journal of China University of Mining and Technology* **44**, 1100–9 (in Chinese with English abstract).

Milliken KL and Laubach SE (2000) Brittle deformation in sandstone diagenesis as revealed by scanned cathodoluminescence imaging with application to characterization of fractured reservoirs. In *Cathodoluminescence in Geosciences* (eds M Pagel, V Barbin, P Blanc and D Ohnenstetter), pp. 225–43. Berlin: Springer-Verlag.

Mogi K (1962) Study of elastic shocks caused by the fracture of heterogeneous materials and their relation to earthquake phenomena. *Bulletin of the Earthquake Research Institute, University of Tokyo* **40**, 125–73.

Nelson RA (2001) *Geological Analysis of Naturally Fractured Reservoirs.* Houston, TX: Gulf Publishing Company, 13 pp.

Neng Y, Xie HW, Sun TR, Lei GL and Xu LL (2013) Structural characteristics of Keshen segmentation in Kelasu structural belt and its petroleum geological significance. *Petroleum Geology* **2**, 1–6 (in Chinese with English abstract).

Nian, T, Wang GW, Xiao CW, Zhou L, Sun YH and Song HY (2016) Determination of in-situ stress orientation and subsurface fracture analysis from image-core integration: an example from ultra-deep tight sandstone (BSJQK Formation) in the Kelasu Belt, Tarim Basin. *Journal of Petroleum Science and Engineering* **147**, 495–503.

Pi XJ, Xie HW, Zhang C, Tian ZJ and Zou HY (2002) Mechanisms of abnormal overpressure generation in Kuqa foreland thrust belt and their impacts on oil and gas reservoir formation. *Chinese Science Bulletin* **47**, 84–90 (in Chinese with English abstract).

Pollard DD and Aydin A (1988) Progress in understanding jointing over the past century. *GSA Bulletin* **100**, 1181–204.

Pruess K (1983) Heat transfer in fractured geothermal reservoirs with boiling. *Water Resources Research* **19**, 201–8.

Qu HZ, Zhang FX, Wang ZY, Yang XT, Liu HT, Ba D and Wang Q (2016) Quantitative fracture evaluation method based on core-image logging: a case study of Cretaceous Bashijiqike Formation in KS2 well area, Kuqa Depression, Tarim Basin, NW China. *Petroleum Exploration and Development* **43**, 1–8.

Schlumberger (2015) Imaging: getting the picture downhole. *Oilfield Review* **27**, 4–56.

Secor DT (1965) Role of fluid pressure in jointing. *American Journal of Science* **263**, 633–46.

Secor DT (1969) Mechanics of natural extension fracturing at depth in the earth's crust. In *Research in Tectonics* (eds AJ Baer and DK Norris), pp. 3–47. Ottawa: Geological Survey of Canada Paper 52–68.

Shaik AR, Rahman SS, Tran NH and Tran T (2011) Numerical simulation of fluid rock coupling heat transfer in naturally fractured geothermal system. *Applied Thermal Engineering* **31**, 1600–6.

Shou JF, Zhu GH and Zhang HL (2003) Lateral structure compression and its influence on sandstone diagenesis: a case study from the Tarim basin. *Acta Sedimentologica Sinica* **21**, 90–5 (in Chinese with English abstract).

Simmon G and Richter D (1976) Microcracks in rock. In *The Physics and Chemistry of Minerals and Rocks* (eds RGJ Strens), pp. 105–37. Chichester: Wiley.

Solano N, Zambrano L and Aguilera R (2011) Cumulative-gas-production distribution on the Nikanassin Formation, Alberta and British Columbia, Canada. *SPE Reservoir Evaluation and Engineering* **14**, 357–76.

Stearns DW and Friedman M (1972) Reservoirs in fractured rock. In *Stratigraphic Oil and Gas Fields – Classification, Exploration Methods, and Case Histories* (ed. RE King), pp. 82–106. AAPG Memoir 16 / SEG Special Publication 10.

Stearns DW (1968) Certain aspects of fracture in naturally deformed rocks. In *NSF Advanced Science Seminar in Rock Mechanics* (eds RE Rieker), pp. 97–118. Bedford: Air Force Cambridge Research Laboratories, Special report AD669375I.

Sun XW, Hou GT, Yu X, Wei HX, Mo T, Zhou L, Xie YN and Luo HN (2015) Model for the fracture development of the sand with low-permeability in the foreland faulted fold belt. *Geotectonica et Metallogenia* **39**, 808–15.

Tavani S, Storti F, Lacombe O, Corradetti A, Muñoz JA and Mazzoli S (2015) A review of deformation pattern templates in foreland basin systems and fold-and-thrust belts: implications for the state of stress in the frontal regions of thrust wedges. *Earth-Science Reviews* **141**, 82–104.

Tham LG, Liu H, Tang CA, Lee PKK and Tsui Y (2005) On tension failure of 2-D rock specimens and associated acoustic emission. *Rock Mechanics and Rock Engineering* **38**, 1–19.

Ukar, E, Laubach SE, Hooker JN (2019) Outcrops as guides to subsurface natural fractures: example from the Nikanassin Formation tight-gas sandstone, Grande Cache, Alberta foothills, Canada. *Marine and Petroleum Geology* **103**, 255–75.

Vermilye JM and Scholz CH (1995) Relation between vein length and aperture. *Journal of Structural Geology* **17**, 423–34.

Wang JP, Zhang RH, Zhao JL, Wang K, Wang B, Zeng QL and Liu C (2014) Characteristics and evaluation of fractures in ultra-deep tight sandstone reservoir. *Natural Gas Geoscience* **25**, 1735–45 (in Chinese with English abstract).

Wang X, Jia CZ, Yang SF, Aurelia HF and John S (2002) The time of deformation on the Kuqa fold-and-thrust belt in the Southern Tianshan – based on the Kuqa river area. *Acta Geologica Sinica* **76**, 55–63 (in Chinese with English abstract).

Wang X, Li Y, Lv XX, Wang Y, Zhou L, Zhuo QG and Shang JW (2015) Characteristics of formation pressure and its significance for the subsalt deep layer in foreland thrust belt of Kuqa Depression. *Chinese Journal of Geology* **50**, 1200–7 (in Chinese with English abstract).

Wang ZM (2014) Formation mechanism and enrichment regularities of Kelasu subsalt deep large gas field in Kuqa Depression, Tarim basin. *Natural Gas Geoscience* **25**, 153–66 (in Chinese with English abstract).

Wang ZM and Long HS (2010) Different hydrocarbon accumulation histories in the Kelasu-Yiqikelike structural belt of the Kuqa foreland basin. *Acta Geologica Sinica (English edition)* **84**, 1195–208.

Wang ZY, Liu C, Zhang YF, Qu HZ, Yang XT and Liu HT (2016) A study of fracture development, controlling factor and property modelling of deep-lying tight sandstone in Cretaceous thrust belt K region of Kuqa Depression. *Acta Petrologica Sinica* **32**, 865–76 (in Chinese with English abstract).

Yang F, Zhu CQ, Wang XH, Qu HZ, Zhang FX and Niu XN (2013) A capacity prediction model for the low porosity fractured reservoirs in the Kuqa foreland basin, NW China. *Petroleum Exploration and Development* **40**, 341–5.

Yuan J, Yang XJ, Yuan LR, Cheng RH, Zhu ZQ, Li CT and Dong DT (2015) Cementation and its relationship with tectonic fractures of Cretaceous sandstones in DB gas field of Kuqa sub-basin. *Acta Sedimentologica Sinica* **33**, 754–63 (in Chinese with English abstract).

Zeng LB and Li XY (2009) Fractures in sandstone reservoirs with ultra-low permeability: a case study of the Upper Triassic Yanchang Formation in the Ordos Basin, China. *AAPG Bulletin* **93**, 461–77.

Zeng LB and Liu BM (2006) Overpressure in Kuqa Foreland Thrust Zone, Tarim Basin, NW China: Origin and its impacts on hydrocarbon accumulation. *Progress in Natural Science* **16**, 1307–1314.

Zeng LB, Tan CX and Zhang ML (2004) Stress field and its effect on hydrocarbon migration in Mesozoic and Cenozoic, Kuqa Depression, Tarim Basin. *Science China Earth Science* **34**, 98–106.

Zeng LB (2010) Microfracturing in the Upper Triassic Sichuan Basin tight-gas sandstones: tectonic, overpressure, and diagenetic origins. *AAPG Bulletin* **94**, 1811–25.

Zhang FX, Wang XH, Li Y, Niu XN and Qin SY (2011) The contribution of fractures of Kuqa foreland fractured sandstone reservoirs to formation permeability. *Journal of Oil and Gas Technology* **33**, 149–52 (in Chinese with English abstract).

Zhang HL, Zhang RH, Yang HJ, Yao SG and Ma YJ (2012) Quantitative evaluation methods and applications of tectonic fracture developed sand reservoir: a Cretaceous example from Kuqa foreland basin. *Acta Petrologica Sinica* **28**, 827–35 (in Chinese with English abstract).

Zhang RH, Zhang HL, Ma YJ, Shen Y, Li C and Zhang LJ (2008) Origin of extra low porosity and permeability high production reservoirs: a case from Bashijiqike reservoirs of Dabei1 oil field, Kuqa Depression. *Natural Gas Geoscience* **19**, 75–82 (in Chinese with English abstract).

Zhang RH, Yang HJ, Wang JP, Shou JF, Zeng QL and Liu Q (2014) The formation mechanism and exploration significance of ultra-deep, low-porosity and tight sandstone reservoirs in Kuqa Depression, Tarim Basin. *Acta Petrolei Sinica* **35**, 1057–69 (in Chinese with English abstract).

Zhang ZP, Lin W and Wang QC (2003) Progressive structural evolution of Kelasu-Yiqikelike Structural Belt in Kuqa Depression. *Geotectonica et Metallogenia* **27**, 327–36.

Zhao MJ, Lu SF and Li J (2002) The geochemical features of natural gas in Kuqa Depression and the discussion on the gas source. *Petroleum Exploration and Development* **29**, 4–7 (in Chinese with English abstract).

Zhao WZ, Wang HJ, Shan JZ, Wang ZY, Zhao CY and Wang ZC (2005) Analysis of highly efficient gas reservoiring process in Kuqa Depression. *Oil and Gas Geology* **26**, 703–10 (in Chinese with English abstract).

Zhu YX, Guo QY, Shao XJ, Song WJ, Fu JK and Li DM (2000) Study on reservoir sedimentary facies of the Cretaceous in the north of Kuqa Depression. *Journal of Palaeogeography* **2**, 58–65 (in Chinese with English abstract).